FEATURE ARTICLE

New Insights for Self-Assembled Monolayers of Organothiols on Au(111) Revealed by Scanning Tunneling Microscopy

Guohua Yang and Gang-yu Liu*

Department of Chemistry, University of California, Davis, California 95616

Received: August 29, 2002; In Final Form: May 5, 2003

In the past decade, scanning tunneling microscopy (STM) has revealed new information regarding self-assembled monolayers (SAMs) of organothiols on Au(111) at the molecular level. The periodicity, defects, morphology, and various phases during the self-assembly process have been visualized with unprecedented detail. Using STM under ultrahigh vacuum, new insights regarding SAMs have been revealed from the perspective of potential applications in molecular devices. This article focuses on a molecular-level understanding of the formation of adatom and vacancy islands and reveals how the structure is impacted by introducing aromatic termini. The thermal stability and thermally induced structural evolution of SAMs are monitored in situ. The behavior of alkanethiol molecules under local electric field and tunneling current are studied with molecular resolution. Molecular-level insight regarding negative differential resistance of SAMs is also discussed.

I. Introduction

Self-assembled monolayers (SAMs) on metal surfaces have attracted much attention in recent years, motivated by their potential applications in molecular electronic devices,[1−4] microelectromechanical and nanoelectromechanical systems (MEMS and NEMS, respectively),[5−9] chemical and biosensors,[10−13] and in the control of biomolecular adhesion on surfaces.[14−20] As the feature size in complementary metal oxide semiconductor (CMOS) systems, biochips, and MEMS continues to miniaturize, researchers turn to organic monolayers as alternatives for coatings and the active component at interfaces. The incorporation of organic molecules provides a new mechanism to tailor interfacial properties without introducing bulky materials. The desired interfacial properties, such as lubricity, protein adhesion, and electron transfer, may be regulated by incorporating various functional groups within organic molecules.[13,21−24] How to design and synthesize the proper organic molecules, and then how to incorporate them into devices, in the form of monolayers, nanostructures, or microstructures with the desired properties, are key issues in realizing the promising potentials of SAMs.

A fundamental approach is to investigate the structure, packing, stability, and interfacial properties of SAMs at the molecular level, which has been our research focus during the past few years. *Alkanethiol SAMs provide an ideal starting point, as well as a model system, for organic monolayers and thin films.* The structure of alkanethiol SAMs has been studied using various techniques, including spectroscopy, diffraction, and microscopy.[25−27] Among these investigations, scanning tunneling microscopy (STM) provides a visual picture at the atomic and molecular level.[28−30] Figure 1 includes two STM topographs acquired in our laboratory that illustrate the well-known morphology, structure, and packing of decanethiol SAMs. As revealed in Figure 1A, decanethiol molecules form ordered domains on Au(111) surfaces, which are separated by domain boundaries, Au(111) steps, and a large number of pitlike depressions with average diameters of 2−5 nm and a depth of 0.24 nm. These depressions are called "etch pits" or gold vacancy islands.[31−36] Further discussion regarding the formation of gold vacancy islands will be addressed in section III of this article. At the molecular level, alkanethiols form a well-ordered, closely packed structure with a fundamental periodicity of ($\sqrt{3} \times \sqrt{3}$)R30° with respect to Au(111) (see Figure 1C). Using diffraction,[37,38] or with higher-resolution STM[39,40] studies, a $c(4\sqrt{3} \times 2\sqrt{3})$R30° superlattice is revealed, as shown in Figure 1B and C. The alkyl chains are tilted from the surface normal by ∼30°, according to IR[41,42] and X-ray[43] experiments. The closely packed structure of long-chain alkanethiols is the foundation of many known properties and applications of these simplest SAMs, such as passivation,[44,45] lubrication,[46−48] antistiction in MEMS,[49,50] electron-transfer barriers,[51−54] and resists for microlithography and nanolithography.[55−61]

For the design and development of SAM-based devices, a fundamental understanding and correlation of the structure and electronic properties, as well as the thermal stability, are essential. Using STM under ultrahigh vacuum (UHV), we have investigated structures at the molecular level and correlated them with the thermal stability of alkanethiol SAMs. In addition, STM-tip−SAM contact has been used to effectively mimic the interfaces within SAM-based electronic devices, such as rectifiers,[62,63] molecular switches,[64,65] and single electron tunneling devices.[66,67] In these setups, STM spectroscopy, such as current−voltage ($I-V$) and current−distance ($I-Z$) measurements, reveals specific information regarding the electronic behavior at the interface. Information from our research provides

* Author to whom correspondence should be addressed. E-mail: liu@chem.ucdavis.edu.

10.1021/jp0219810 CCC: $25.00
Published on Web 07/26/2003

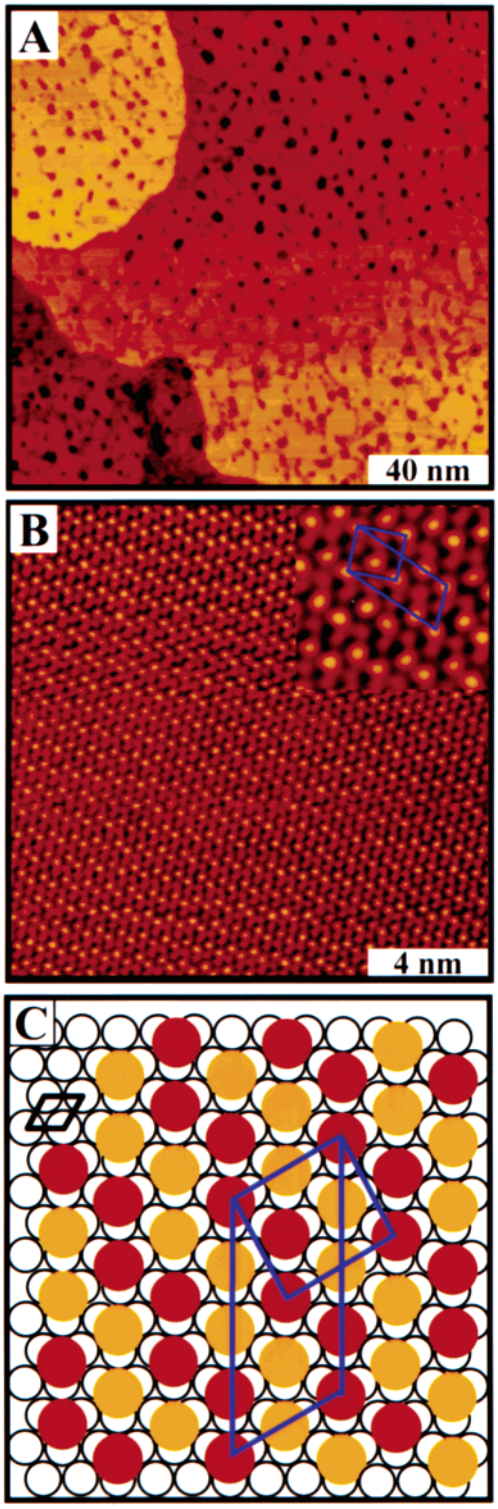

Figure 1. Characteristic morphology of decanethiol SAMs on Au(111). Panel A shows a 200 nm × 200 nm STM topograph; the dark pits are vacancy islands, and the dark lines correspond to domain boundaries. Panel B shows a 20 nm × 20 nm topograph taken after the sample was annealed at 350 K for 4 h; the primitive rectangular unit cell and the $c(4\sqrt{3} \times 2\sqrt{3})$ superlattice (abbreviated as $c(4 \times 2)$) are indicated in the inset. Panel C shows a schematic diagram illustrating the lattice structure and unit cells of alkanethiol SAMs on Au(111).

new scientific insight regarding the molecular-level structure and defects, the impact of introducing specific functional groups, and the behavior of SAMs under heating, a local electrical field, and tunneling current. The study of adsorbates under a local electric field and tunneling current also sheds light on the mechanism of molecular manipulation.

II. Experimental Section

The primary tool employed for our investigations is an UHV STM apparatus (RHK Technology, Inc),[68,69] which has a base pressure of 2×10^{-10} Torr. A variable-temperature sample stage is available for thermal stability studies. The UHV system has a rapid-entry load-lock for sample and tip exchanges. The chamber is also equipped with a quadrupole mass spectrometer, an ion gun, and a sample/tip storage manipulator.

All STM images were acquired in a high-impedance, constant-current mode. Typical imaging conditions for different thiol SAMs are bias voltages of $V = \pm 0.5$ to ± 2.0 V and a tunneling current of $I = 1-100$ pA. The STM tips used for these studies are tungsten wires that were cut under ambient conditions and then electrochemically etched. A homemade electrochemical potentiostat was used to automatically monitor and stop the etching process when the current dropped below the setpoint. Typically, tips were etched at 2.1 V, in a 3 M KOH solution. STM piezoelectric scanners were calibrated laterally, with graphite(0001) and Au(111), and vertically, using the height of the Au(111) steps (2.35 Å). Calibrations were further verified by the periodicity of decanethiol SAMs on Au(111).

The Au(111) samples (Alfa Aesar, 99.99%) were prepared by thermally depositing gold onto freshly cleaved mica substrates in a high-vacuum evaporator (Denton Vacuum, Inc., model DV502-A) at a base pressure of $<1 \times 10^{-6}$ Torr. The mica was preheated to 350 °C. An evaporation rate of 0.3 nm/s was applied until the thickness of the gold thin films reached 200 nm. The films were then annealed at 350 °C for 30 min after deposition, to produce flat Au(111) terraces with an area as large as 200 nm × 200 nm, according to our STM and AFM measurements. The terraces exhibit the well-known $(23 \times \sqrt{3})$ gold reconstruction.[70,71]

Commercially available organothiols (hexanethiol, octanethiol, decanethiol, dodecanethiol, benzenethiol, 1-phenylmethylthiol, 2-phenylethylthiol, and 3-phenylpropylthiol) were used as received, and compounds of 4-chloro-4′-mercaptobiphenyl[69] and 4-[4′-(phenylethynyl)-phenylethynyl]-benzenethiol[72−74] were synthesized following previous procedures. Freshly prepared gold surfaces were immersed in dilute thiol solutions (0.001−1 mM) in ethanol (for alkanethiols) or in dichloromethane (for arenethiols) for at least 24 h. The samples were washed sequentially with pure ethanol and hexane for alkanethiol, or with pure dichloromethane and ethanol for arenethiol before transfer into the UHV system.

Annealing experiments were accomplished using a filament heater that was mounted underneath the sample stage. High temperatures and heating rates were regulated by varying the current. Temperatures were monitored via two thermocouples: one was installed directly underneath the sample, and the other was attached to the sample stage. A typical rate of 0.3 K/min was used for annealing.[75]

The relative tip−sample separation (Z) was determined from $I-Z$ measurements. The zero separation is defined as the tip−methyl contact, which can be identified easily as the ln $I-Z$ curves begin to change their slopes. The actual separation can be calculated from the approaching distance from the initial position to the contact point. The penetration distance is extracted from the approaching distance from the contact position to the final position. $I-V$ measurements were acquired according to the following systematic steps. First, alkanethiol

SAMs on Au(111) were imaged at a bias voltage of 1 V and a tunneling current of 5−30 pA, to reveal domains containing the $c(4\sqrt{3} \times 2\sqrt{3})R30°$ superlattice. The STM tip was then parked at a designated location, where systematic $I-V$ measurements could be acquired, above a thiol molecule within an ordered domain. We emphasize that all the $I-V$ curves shown in this article were acquired when the tip was in contact with the surface of the SAMs. The same area was imaged again after $I-V$ measurements.

III. Formation Mechanism of Gold Vacancy and Adatom Islands

Historical accounts of the observation of vacancy islands have been previously reviewed.[30,34] In the latest and widely accepted model proposed by Poirier,[34] the mechanism of forming vacancy islands was based on UHV−STM studies of gas-phase deposition of alkanethiols on Au(111) surfaces. The model proposes a relaxation-mediated, in-plane gold redistribution process. A clean, bare Au(111) surface exhibits a herringbone morphology of $(23 \times \sqrt{3})$ reconstruction, which can be understood as *one* extra Au atom per $(23 \times \sqrt{3})$ unit cell, or 4.4% compression (or higher density), with respect to the bulk gold crystal.[70,71,76] During alkanethiol chemisorption processes, the reconstruction is lifted and *two* atoms per $(23 \times \sqrt{3})$ primitive unit cell are released on the surface terraces, thus producing one net vacancy per primitive unit cell. The released Au adatoms diffuse rapidly and merge at neighboring step edges while the vacancies nucleate and coalesce into vacancy islands in the terraces. This model successfully explains most of the experimental observations for alkanethiols on Au(111).[34]

Two observations from previous work and our recent investigations indicate that refinement of this model is necessary. First, in Poirier's model, the initial process involves the release of two Au atoms instead of one. However, the driving force for the simultaneous release of extra Au adatoms and the subsequent formation of Au vacancies is not clear. Second, STM investigations[68,69,77−80] indicate that arenethiol SAMs exhibit very few vacancy islands, in contrast to alkanethiol SAMs on gold.[34] In Figure 2, STM topographic images of seven thiol SAMs on Au(111) surfaces are shown. The images seem to fall into two categories, according to the characteristics of gold vacancy and adatom islands. The images in the left-hand column of the figure represent alkanethiols and aromatic-terminated aliphatic thiol SAMs, which include decanethiol (Figure 2A), 1-phenyl-methanethiol (Figure 2B), 2-phenyl-ethanethiol (Figure 2C), and 3-phenyl-propanethiol (Figure 2D). All these SAMs show morphologies and structures similar to that of the normal alkanethiols;[30] i.e., the monolayer surfaces consist of domains of closely packed thiol molecules decorated with vacancy islands at the domain boundaries. In comparison to alkanethiol, 2-phenyl-ethanethiol (Figure 2C) has fewer and larger vacancy islands, with an average size of 5−15 nm. The depth of these vacancy islands is 2.4 Å, which is consistent with the expected height of a Au(111) single atomic step. The images in the right-hand column of the figure are arenethiol SAMs on Au(111): benzenethiol (Figure 2E), 4-chloro-4′-mercaptobiphenyl (Figure 2F), and 4-[4′-(phenylethynyl)-phenylethynyl]-benzenethiol (Figure 2G). In contrast to alkanethiol SAMs, vacancy islands in arenethiol SAMs are sparser in number and density. Instead, small adatom islands with lateral dimensions of 1−15 nm are abundant. These adatom islands are located on the Au(111) terraces with a measured height of 0.24 nm, which is consistent with the theoretical height of a single gold layer with individual Au atoms sitting on the triple hollow sites of the Au(111) surface. Arenethiol molecules cover the surface of Au adatom islands, resulting in the morphology observed in Figure 2E−G.

The diffusion-mediated relaxation model cannot account for the adatom islands, nor can it account for the low population of vacancy islands observed for arenethiols. We have carefully analyzed the existing experimental evidence and conducted a series of systematic STM studies of gold vacancy and adatom islands, including the results shown in Figure 2. The evidence collectively enables us to refine Poirier's model, to propose a new mechanism (schematically shown in Figure 3) that accounts for all experimental evidence, including the two observations that have been discussed.

First, as noted by Poirier, the evolution of surface structure and the mobility of surface atoms during the formation of SAMs is critical in understanding the mechanism of forming gold vacancy and adatom islands.[34] Previous experimental evidence including our own observations can be summarized as follows. Clean, bare Au(111) surfaces adopt a unique $(23 \times \sqrt{3})$ reconstruction, with respect to the bulk (111) planes, because the binding symmetry is broken for surface atoms.[30,70,71,76] The reconstructed Au(111) surface is characterized by a 4.4% lateral compression, relative to the bulk layers, i.e., one extra Au atom per unit cell.[76] Reconstruction leads to variations in registry between the top surface and the atomic layers below, such that the stacking arrangement alternates between unfaulted *ABC* stacking and faulted *ABA* stacking.[30,70] These faulted and unfaulted regions are separated by rows of bridging Au atoms. To further reduce surface tension, the paired ridges form hyperdomains that are characterized by alternating 60° and 120° turns.[30,71] In STM topographs, a unique morphology with zigzag ridges are shown.[71] For the model shown in Figure 3A, a reconstructed Au(111) surface is represented by shading to differentiate its structure from the bulk. The extra surface atoms or reconstruction are essential for the formation of gold vacancy islands and adatom islands. STM studies of alkanethiol SAMs on other noble metals, such as Ag(111)[81] and Cu(111),[82] have not shown the presence of vacancy nor adatom islands, because these metal surfaces do not have compressive reconstructions. Alkanethiol adsorption on the reconstructed Au(001), on the other hand, does exhibit vacancy and adatom island features.[83] Surfaces of Au(001) have a (5×20) reconstruction, corresponding to the presence of 26% extra surface atoms.[84,85]

Second, the gold surface morphology constantly evolves during the adsorption of thiols.[34,86−89] The zigzag or herringbone features, characteristic of $(\sqrt{3} \times 23)$ reconstruction, disappear in the regions of thiol adsorption, whereas the surface morphology of uncovered areas also changes accordingly.[34,87] The removal of reconstruction is the result of releasing extra Au atoms, i.e., adatom islands observed experimentally by UHV STM of gas-phase deposition of thiol molecules.[34] Vacancy islands also become visible by STM: as the surface reaction proceeds, these islands are mobile during adsorption and coalesce into larger islands.[34] The mobility of the vacancy islands are regulated by temperature, thiol concentration, structural coverage, and the chain length of the molecules.[33,34] For example, at room temperature, the density of gold vacancy islands is high, with a small average size, when self-assembly occurs at high thiol concentration. In the case of low-coverage structures such as striped phases, fewer and larger vacancy and adatom islands are present, in comparison to a saturated SAM (see Figure 1C and Figure 1 in ref 34).

Third, after the alkanethiol molecules have fully covered the Au(111) surface, the surface reconstruction is lifted completely.

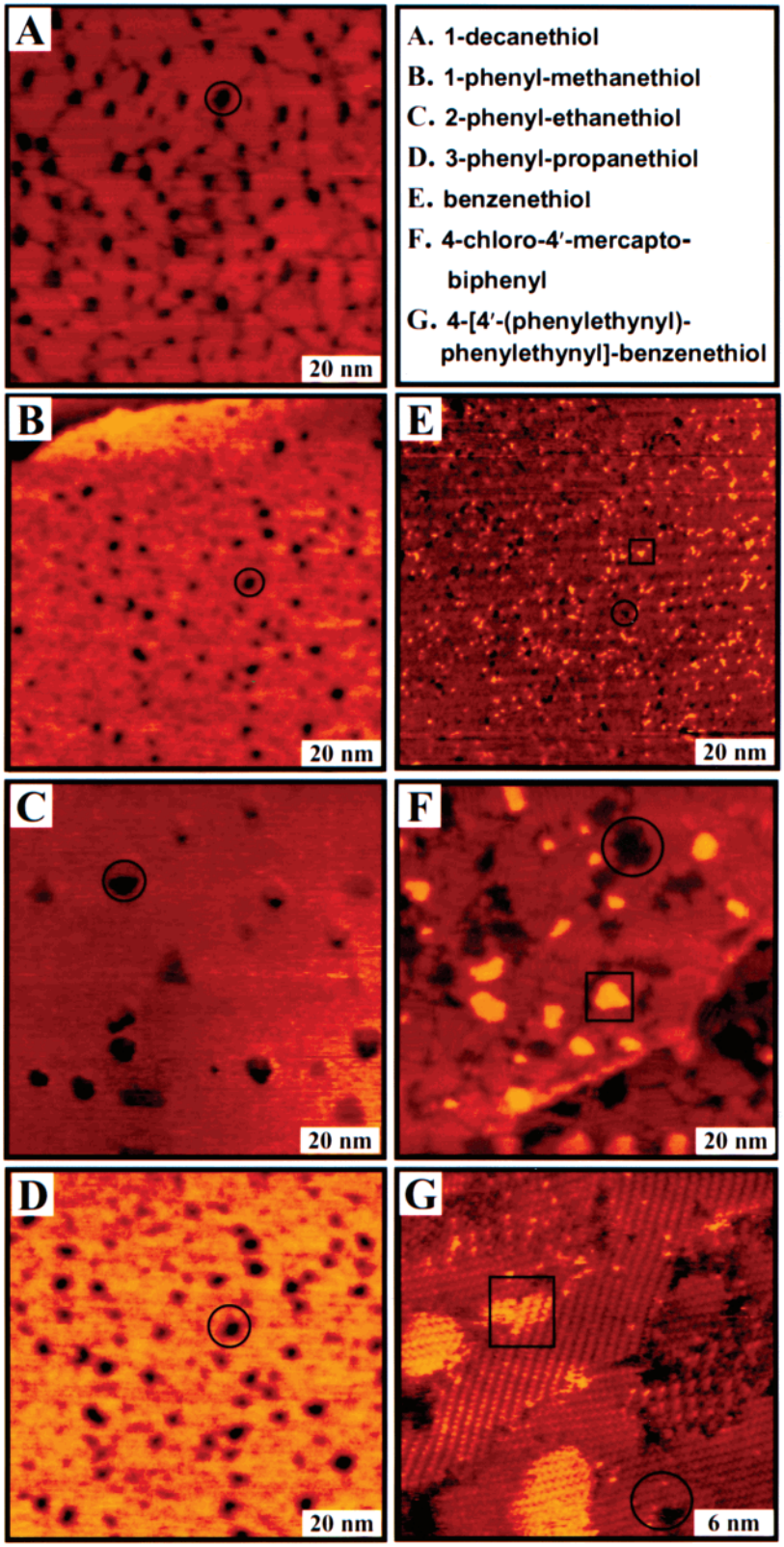

Figure 2. Morphologies of thiol SAMs on Au(111). Molecules include (A) decanethiol, (B) 1-phenyl-methanethiol, (C) 2-phenyl-ethanethiol, (D) 3-phenyl-propanethiol, (E) benzenethiol, (F) 4-chloro-4′-mercaptobiphenyl, and (G) 4-[4′-(phenylethynyl)-phenylethynyl]-benzenethiol. Examples of gold vacancy and adatom islands are highlighted by circles and squares, respectively.

This conclusion is supported by observation of a commensurate $(4\sqrt{3} \times 2\sqrt{3})R30°$ structure of SAMs on Au(111), as measured by grazing-incidence X-ray diffraction (GIXD),[38,90] low-energy atom diffraction (LEAD),[37] and STM experiments.[39,40] Flat terraces of bare Au(111) exhibit a large number of vacancy islands at saturation coverage. In most cases, the defects do not appear near Au step edges and are quite small (1−5 nm), with a narrow size distribution. STM observations indicate that most of the vacancy and the adatom islands are located at domain boundaries in SAMs on Au(111) terraces.[33,39,40,91−93]

Fourth, the structural evolution, in terms of the size and distribution of etch pits, seems to slow significantly or cease

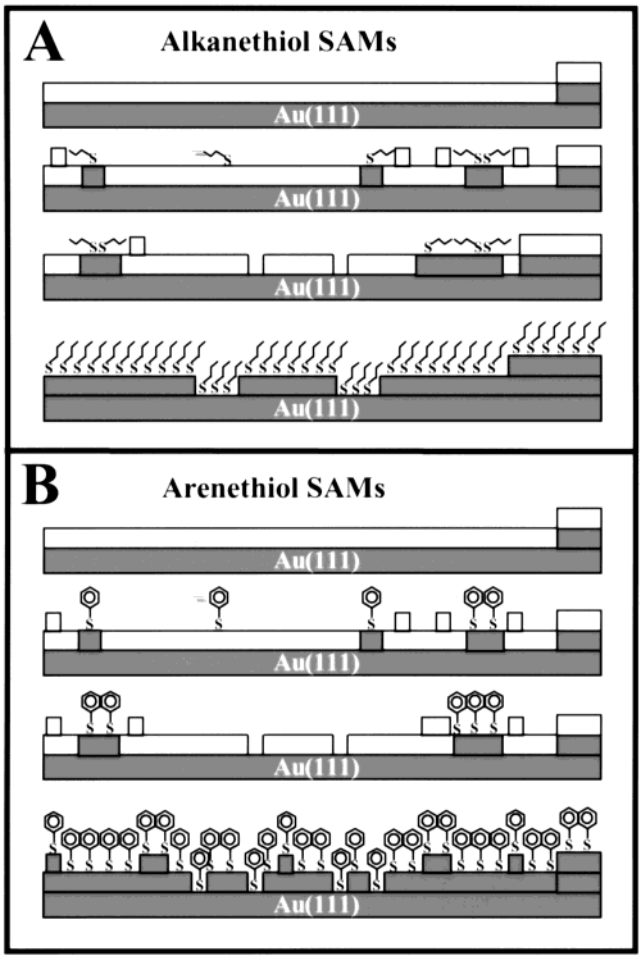

Figure 3. Proposed models of gold vacancy and adatom island formation during the self-assembly of (A) alkanethiol and (B) arenethiol on Au(111). Bulk gold crystal is represented as shaded regions, whereas reconstructed Au(111) surface regions are represented as blocked white areas.

once the surface coverage reaches a monolayer, indicating that the mobility of vacancy islands is insignificant in the presence of SAMs at room temperature (kinetically frozen). Upon annealing at elevated temperatures, vacancy islands will combine into larger islands, as shown in Figure 4. The highly dispersed vacancy islands have a large perimeter-length-to-area ratio. A coarsening process of the vacancy islands is consistent with the Ostwald ripening process, as also revealed by several other groups.[94,95] Ostwald ripening is characterized by the growth of large features at the expense of small ones. Ripening of the vacancy island is driven by the tendency to reduce the overall boundary tension or step-edge energy. We and others have shown that the coarsening of vacancy islands can be accelerated at elevated temperatures.[74,92,95−98]

Finally, from our recent STM investigations, aliphatic thiol SAMs on Au(111) have a distinctly different morphology from that of arenethiol SAMs, as shown in Figure 2. For arenethiol SAMs on Au(111), absorbate molecules cover both the Au(111) terraces and the Au adatom islands. In addition, annealing arenethiol SAMs under the same conditions as alkanethiols does not result in observable morphological changes, in terms of pits and adatom island coalitions, suggesting that the mobility of Au adatoms and vacancy islands is significantly less during the formation of arenethiol SAMs than in alkanethiol SAMs.

Analyzing all the experimental evidence, we have modified the relaxation-mediated, in-plane gold redistribution model[34] and propose two new models, as schematically shown in Figure 3A and B, to illustrate the adsorption of alkanethiol and arenethiol molecules, respectively. Clean Au(111) surfaces (e.g., in an UHV environment) adopt a distinct ($\sqrt{3} \times 23$) herringbone reconstruction. Each ($\sqrt{3} \times 23$) unit cell contains two excess Au atoms (a total of 46 Au atoms), giving rise to a surface compression of 4.4%. Initial adsorption of thiols resulted in gas-phase formation or physisorption, which is mobile.[34,87−89] Domains of horizontal phase follow, where chemisorption occurs. Upon chemisorption of the S atom onto, for example, a triple hollow site in the bridging or faulted regions, the sulfur expanded the separation of the three Au atoms underneath toward the unreconstructed Au(111) structure. Regardless of the orientation of thiols—vertical or horizontal—such local perturbation is present, because of the chemisorption nature of thiols. Increasing the coverage results in accumulation of this local structural perturbation.

Such local perturbations induce two main events. First, Au atoms were ejected at the nearby sulfur adsorption sites, to release the compression in the reconstructed structure. These ejected Au atoms would diffuse rapidly on the surface, even at room temperature, and merge at the surrounding step edges (see Figure 3A), which is energetically more favorable than individual Au atoms above the surfaces. In the case of alkanethiol adsorption, such diffusion can occur in the bare and thiol-covered regions. Therefore, one has hardly observed adatomic islands in alkanethiol SAMs. *Second, single thiols (both physisorbed and chemisorbed thiols) can diffuse laterally until they nucleate at neighboring larger thiol domains*. In the meantime, the surface Au atoms move or reorganize to accomplish the following: (i) regain the ($\sqrt{3} \times 23$) structure in the area uncovered by thiol; (ii) maximize the domain size in the uncovered region (local annealing due to chemisorption); and (iii) regain the bulk Au(111) structure in the thiol-covered regions. Observation of the migration of the herringbone structure supports the concept of these reorganization processes (see Figure 7 in ref 34).

We have identified at least two main sources for the formation of vacancy islands. First, the number of extra Au atoms uplifted during the initial thiol adsorption is dependent on the adsorption sites and the density of the thiols. For physisorbed thiols, when they combine at neighboring larger thiol domains and become chemisorbed above the bridging sites of the Au herringbone reconstruction, the underlying gold surface relaxes, resulting in the release of two extra Au atoms onto the terracce. For single chemisorbed thiols, the extra Au atoms of the underlying reconstruction have already been ejected onto the terrace during the initial chemisorption. In both cases, there are insufficient numbers of Au atoms in the uncovered regions to sustain the ($\sqrt{3} \times 23$) structure as a single two-dimensional (2D) crystal. Second, chemisorbed thiol molecules may still be mobile on the surface, which leaves the original binding sites unable to maintain the ($\sqrt{3} \times 23$) structure. Therefore, the bare surface reorganizes into a new morphology, i.e., ($\sqrt{3} \times 23$) structure domains that are punctuated by gold vacancies.

The vacancy defects on gold are mobile, creating the vacancy islands observed in SAMs. Such motion is often accompanied by reorganization of the herringbone structure in the uncovered region. In contrast, adatoms released in the self-assembly process diffuse rapidly and merge at neighboring step edges; thus, adatom islands are not visible in alkanethiol SAMs. Both experimental results and molecular dynamics simulations suggest that adatoms on metal (111)-oriented face-centered cubic (fcc(111)) surfaces have much smaller energy barriers (E_d) for

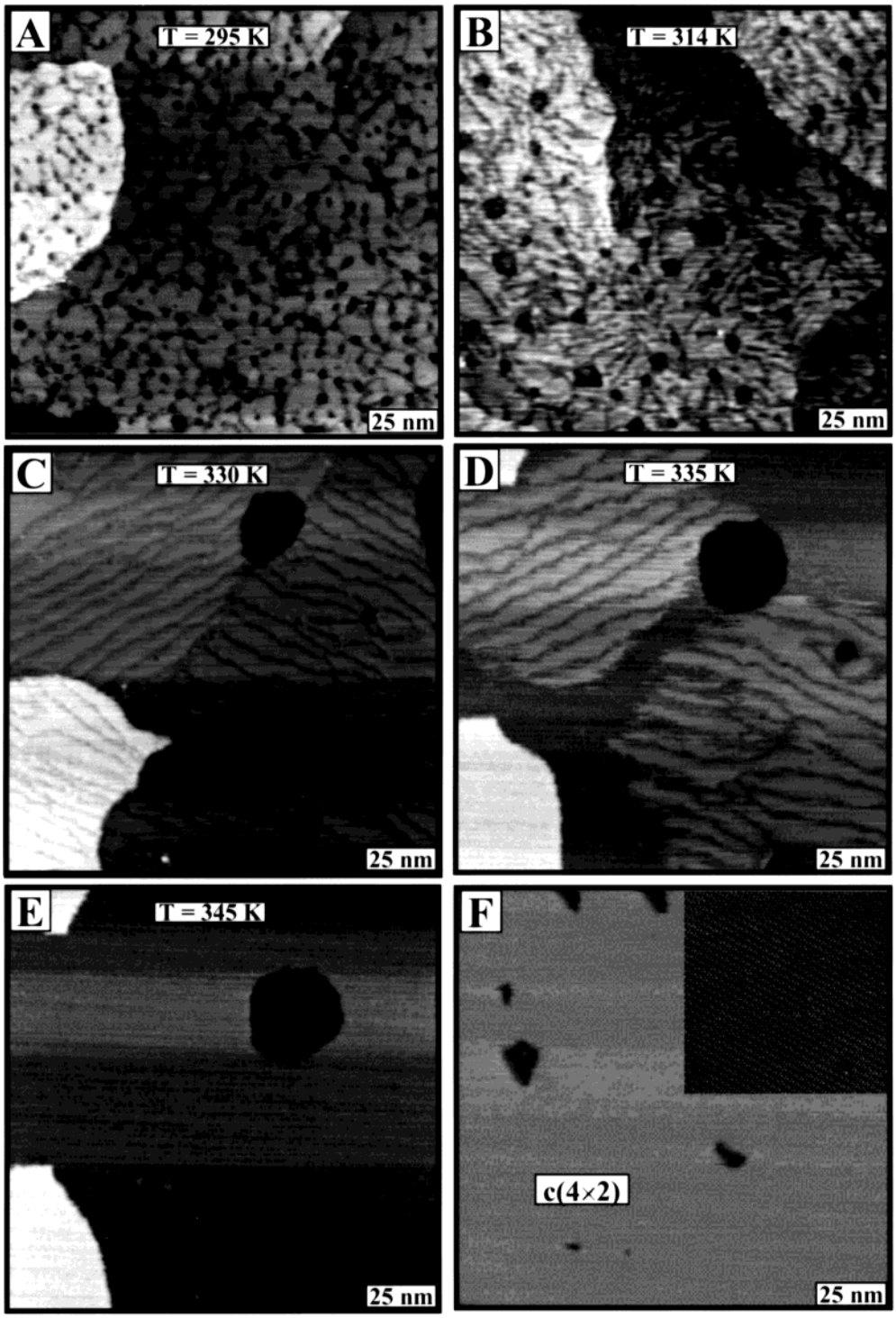

Figure 4. In situ snapshots of the evolution of morphology and structure of decanethiol SAMs on Au(111) during annealing: (A) $T = 295$ K, (B) $T = 314$ K, (C) $T = 330$ K, (D) $T = 335$ K, (E) $T = 345$ K, and (F) $T = 350$ K and imaged at 295 K. A liquid phase becomes the dominant structure at 345 ± 5 K.

diffusion than vacancies. For example, in the case of Au(111), $E_d = 0.102$ eV for adatoms, whereas $E_d = 0.455$ eV for vacancies.[99]

For the arenethiol self-assembly process, a similar morphology was anticipated, because of the chemisorptive nature of the sulfur at the gold interface. However, distinct morphologies for arenethiol SAMs are observed, as shown in Figure 2. A proposed model for arenethiols is shown in Figure 3B. During the initial arenethiol adsorption, the surface structural evolution is similar to alkanethiol self-assembly processes. The gold surface reconstruction is lifted in the arenethiol-covered areas, which is accompanied by the release of extra Au atoms. The uncovered region undergoes reorganization, forming small Au vacancies.

The key difference between arenethiol self-assembly and alkanethiol adsorption is that Au adatoms and vacancies have less mobility during arenethiol adsorption than in alkanethiol self-assembly. The lower mobility results in small vacancy islands and the remaining adatom islands in arenethiol SAMs, as shown in Figure 2 and illustrated in Figure 3B. The mobility difference is proven directly by the evolution of the gold surface morphology during mild annealing. Annealing at ~330 K can eliminate almost all small gold vacancy islands for decanethiol

SAMs, as shown in Figure 4C. However, for arenethiol SAMs, at relatively higher temperatures (e.g., annealing at 400 K for 6−10 h), Au adatom and vacancy islands remain unchanged.

The mobility of surface Au atoms reflects the diffusion barrier of surface Au atoms, which is governed by S−Au binding at the interfaces. Surface atoms exhibit less mobility in arenethiol SAMs; therefore, the diffusion barrier is higher in the presence of arenethiol molecules. It has been reported by Sette et al.[98] and Trevor et al.[99] that the chemisorption of electronegative atoms, such as S and Cl, on metal surfaces, can weaken neighboring metal−metal (M−M) bonds, leading to lower diffusion barriers and higher surface-metal mobility. The magnitude of the M−M bond weakening is primarily determined by the coverage of the adsorbate and the strength of the adsorbate−metal (A−M) interaction.[98] In the observations of the low mobility of surface Au atoms during arenethiol adsorption, we infer that the S−Au bond at the arenethiol−gold interface is weaker than that in alkanethiol SAMs.

The difference in binding strength at the interface is consistent with known energetics. First, the S atom in arenethiols is linked to an sp^2-hybridized C atom, whereas the S atom in alkanethiols is linked to an sp^3-hybridized C atom. The pK_a value of benzenethiols is 6−8, which is lower than that of alkanethiols (pK_a = 10−11). In addition, alkanethiols can easily replace arenethiols in exchange reactions, whereas arenethiols only adsorb at the defect sites of alkanethiol SAMs.[100,101] Furthermore, in temperature-programmed desorption (TPD) measurements, the binding energy of the striped phase of hexanethiol[102,103] and benzenethiols[104] is estimated to be 127 and 106 kJ/mol, and the physisorption enthalpies for *n*-hexane and benzene are 53 and 60 kJ/mol, respectively.[105,106] Assuming that the energy is completely additive, the S−Au binding energy in the case of alkanethiol and arenethiol are calculated to be 74 and 46 kJ/mol, respectively.

IV. Structural Evolution of Alkanethiol SAMs during Thermal Annealing

The thermal stability of adsorbates is an important parameter in SAM-based molecular devices. Using STM to monitor the annealing process of SAMs provides an effective means to address the issue of thermal stability at the molecular level. Figure 4 shows snapshots selected from in situ and real-time STM imaging of a decanethiol SAM surface during annealing. At room temperature (Figure 4A), solution-grown decanethiol SAMs exhibit a surface morphology that is characteristic of alkanethiol SAMs, as discussed and summarized in the Introduction.

Up to 330 K (see Figure 4B and C), few significant structural changes occurred, except for the gradual coarsening of SAM domains. The total number of vacancy islands clearly decreased, while their average sizes increased, which is consistent with the Ostwald ripening process.[93−95] Domain boundaries, as observed in Figure 4A, became more difficult to distinguish. Lines with negative contrast became evident (the dark depression lines in Figure 4B). The average widths and depths of these depression lines were 2 and 0.1 nm, respectively. The depression lines are likely caused by missing decanethiol molecules, where neighboring thiol molecules tilt over these defects. When the surface in Figure 4B and C was cooled to room temperature, the $(4\sqrt{3} \times 2\sqrt{3})R30°$ superlattice reappeared without the presence of lower-coverage phases, such as striped phases.[29,92,97]

Annealing at 335−340 K (see Figure 4D) leads to ∼90% disappearance of the vacancy islands, while, in some areas, the SAM melted (e.g., the featureless areas in Figure 4D). The unmelted areas consist of ordered domains that are separated by line depressions, as shown in Figure 4D. Judging from the subsequent STM images as a function of annealing temperature, the vacancy islands disappeared due to the lateral diffusion of Au atoms, e.g., from terraces to step edges**.** In agreement with previous studies,[38,95] the rate of the ripening process of etch pits is greatly enhanced by 2D melting. The apparent height difference between the ordered domain and the melting phase is ∼0.1 nm.

TABLE 1: Two-Dimensional Melting Temperatures (T_m) of Alkanethiol ($CH_3(CH_2)_{n-1}SH$) SAMs on Au(111), Measured by Scanning Tunneling Microscopy (STM)

n	chain length (Å)	T_m (K)
6	11.8	308 ± 5
8	14.4	327 ± 5
10	17.0	345 ± 5
12	19.5	367 ± 5

At 345 K, the entire SAM melts, as shown in Figure 4E. Au(111) surfaces at temperatures of >345 K no longer reveal observable changes, indicating that the monolayer is in a 2D liquid phase. For decanethiol SAMs on Au(111), the melting transition is completed at 345 ± 5 K. If this temperature was maintained for 15 min and the sample was subsequently cooled to room temperature, the monolayers recrystallize into a structure that consists of domains of ordered structures with very few Au vacancies, as shown in Figure 4F. The 2D melting point can thus be determined from STM imaging of the annealing process. The melting process and the liquid phase of SAMs were previously reported by helium diffraction, X-ray reflectivity, and STM experiments.[38,88,107,108] The hydrocarbon chains in the melting process engage in various movements such as liberation and conformational changes; therefore, the entire layer in the 2D liquid phase does not exhibit orientational order at the melting point.

In Figure 4F, the SAM was annealed incrementally to 350 K and subsequently cooled to room temperature, at which point the STM image was obtained. In comparison with the SAMs directly taken from solution (Figures 2A and 4A), the crystallinity of annealed SAMs is increased, as evidenced by the large $(4\sqrt{3} \times 2\sqrt{3})R30°$ domains shown in Figure 4F. These 2D crystals could be as large as the dimension of the gold terrace underneath. The inset in Figure 4F shows a 30 nm × 30 nm zoom-in image with molecular resolution, which reveals the $(4\sqrt{3} \times 2\sqrt{3})R30°$ structure.

The measured melting point for dodecanethiol SAMs is 367 ± 5 K, which is consistent with that reported in GIXD investigations.[38] The dependence of the melting point on the chain length of alkanethiol SAMs is summarized in Table 1. The melting temperature is found to increase as a function of the chain length of alkanethiols. This can be explained by stronger intermolecular interactions with an increasing number of methylene groups. By extrapolation, the melting temperature of butanethiol SAMs is ∼290 K; thus, butanethiols do not form 2D crystals, such as the closely packed $(\sqrt{3} \times \sqrt{3})R30°$ structure on Au(111) at room temperature.[34,109,110]

Higher annealing temperatures initiate thiol desorption, and subsequent cooling to room temperature results in the appearance of striped phases that coexist with the closely packed structure. The periodicity and density of the striped phases are dependent on the annealing conditions. The 2D phase diagram of alkanethiol SAMs have been systematical studied by us[75] as well as other researchers.[27,30,96,109,136]

V. Structure Characterization for SAMs with Phenyl Termini

Organic monolayers allow the formation of a variety of surfaces with the desired interfacial properties of SAMs, by introducing various functional groups. For example, by modifying the terminal group, "Teflon-like" hydrophobic surfaces can be mimicked by introducing CF_3 termini, and hydrophilic surfaces are easily produced via HO- or HOOC-terminated thiols. Mechanical properties such as wetting, friction, lubrication, and adhesion can be modified using SAMs with selected functional groups.[22,48,111−114] Moreover, ferrocene-terminated SAMs provide a platform for fine-tuning electron-transfer properties.[52,53,115] Suitably selected SAMs can tune the effective barrier height of the charge transport at the interface by modifying the permanent dipole layer of SAMs.[74,116,117] Control of the charge injection in SAM-based devices was also reported.[118,119]

To obtain precise control of interfacial properties, especially for device fabrication, a fundamental question must be answered: how does the structure of SAMs change as a result of introducing various functionalities? Conjugated aromatic molecules are promising candidates for molecular electronics.[74,120−122] Although much effort has been devoted to studies of the electron-transport mechanism of conjugated SAM-based devices,[123−130] in situ structural characterization at the molecular level has been relatively unexplored.

We have studied the structure of alkylthiol SAMs with a single phenyl-terminal group per molecule. STM images reveal the structure and morphology of a series of *n*-phenyl-alkylthiol molecules ($C_6H_5(CH_2)_nSH$, referenced as BT_n, where $n = 0-3$). The morphology of benzenethiol (BT_0) is shown in Figure 2E, where a high density of Au vacancies and adatomic islands predominate. High-resolution imaging does not reveal any ordered structures for BT_0.[77,131] Introduction of an alkyl linker between sulfur and benzene dramatically alters the morphology as well as the molecular-level structure, as illustrated in Figures 2B−D and 5. It is difficult to obtain molecular-resolution images for BT_n SAMs, because of the relatively higher defect density and smaller domain size, in comparison to alkanethiol SAMs. For both BT_1 and BT_3, a 2D close-packed structure is clearly recognized in Figure 5A and C. The basic periodicity is 0.50 ± 0.02 nm and 0.51 ± 0.02 nm for BT_1 and BT_3, respectively. The angle between lattice vectors is $58° \pm 5°$ for both SAMs. Therefore, the molecular-level packing of BT_1 and BT_3 SAMs follows the basic $(\sqrt{3} \times 3)R30°$ periodicity on Au(111). These observations are consistent with previous STM and theoretical studies of SAMs of benzyl mercaptan on Au(111).[131] Aromatic groups energetically favor a herringbone structure, based on the intermolecular interactions.[132−134] The herringbone arrangement of BT_1 and BT_3 molecules results in a $(\sqrt{3} \times 2\sqrt{3})R30°$ unit cell on Au(111), as shown in the models of Figure 5A' and C'.

Figure 5B shows a high-resolution image of BT_2. Unlike BT_1 and BT_3 SAMs, BT_2 monolayers exhibit a much larger periodicity, similar to the striped phase. The spacing between stripes is 2.01 ± 0.10 nm, which is 7 times greater than the Au(111) lattice constant. Each stripe shown in Figure 5B is composed of a pair of molecular rows, along which closely packed bright spots are resolved, with separations corresponding to the $\sqrt{3}$ periodicity. These molecular rows align along the $\langle 121 \rangle$ or the next-nearest-neighbor (NNN) direction of Au(111). Previous studies have attributed the bright spots in STM images to the S atoms.[135] Our high-resolution STM images conclude a $(7 \times \sqrt{3})$ (see Figure 5B') lattice for BT_2 SAMs. Each $(7 \times \sqrt{3})$ unit cell contains two BT_2 molecules; thus, the surface coverage of BT_2 is only 50% of that of BT_1 and BT_3 SAMs.

High-resolution structural characterization by STM reveals that the introduction of a phenyl-terminal group impacts both the morphology and molecular-level packing of SAMs. In terms of surface morphology, a higher density of defects, in comparison to normal alkanethiols, is present, because of the relatively bulky size of the phenyl ring, which has a van der Waals dimension of 6.4 Å × 3.3 Å, where the methyl group is 4.5 Å in diameter. It is more difficult to fit the phenyl group into the $(\sqrt{3} \times 3)R30°$ structure (or a nearest-neighbor separation of 5 Å), because of the relatively large and nonspherical shape of the termini. In addition, nearest-neighbor phenyl groups reorient themselves in a herringbone fashion. In terms of molecular-level packing, two outcomes are revealed. First, with an odd number of methylene groups as linkers (such as that with BT_1 and BT_3), thiol molecules form a $(\sqrt{3} \times 2\sqrt{3})R30°$ structure, in which molecules are closely packed. Second, with an even number of methylene groups as linkers (such as that in BT_2), molecules have a tendency to form striped phases instead of a 2D closely packed structure. The periodicity of the striped phase is dependent on the length of the methylene linker. The BT_2 molecules form a $(7 \times \sqrt{3})$ structure on Au(111). Using STM, Duan et al. observed another striped phase for BT_6/Au(111) with a periodicity of 16 Å.[136]

The results described represent an "odd−even" effect, which is an important characteristic of alkanethiol SAMs[137−139] and their derivatives, such as phenyl-terminated SAMs. This effect originates from S−Au bonds at the interface and the orientation of the hydrocarbon chain, with respect to the surface. For $X-(CH_2)_nSH$ molecules (where $n \geq 1$), the sulfur headgroups are connected with sp^3-hybridized C atoms and are chemisorbed strongly to Au(111). The hydrocarbon chains tilt 30° from the surface normal.[140] Therefore, the C−phenyl bonds, as well as the benzene ring, are almost perpendicular to the surface in the case of an odd number of methylene linkers, where a $(\sqrt{3} \times 2\sqrt{3})R30°$ structure is formed with closely packed chains. In contrast, benzene rings are almost parallel to the gold surfaces in the case of an even number of methylene linkers, where the orientation of the benzene rings prohibits the formation of a commensurate $(\sqrt{3} \times 2\sqrt{3})R30°$ structure. Instead, less densely packed structures such as striped phases are observed. The fundamental packing revealed from STM investigations provides a good reference point for SAMs containing phenyl rings.

Analogous "odd versus even" effects were also reported by other researchers. Often, the odd−even effect is sufficiently large to impact the interfacial properties. Lee and co-workers demonstrated an oscillatory behavior when plotting the contact angle versus the chain length of *n*-phenyl-alkanethiol SAMs.[48] SAMs with an odd number of methylene groups exhibit higher contact angles than those obtained with an even number of methylene groups. Rong and co-workers observed oscillations in the contact angle, the packing density, and the tilt angle of the biphenyl moieties for ω-(4′-methyl-4-yl)-alkanethiol ($CH_3-C_6H_4-C_6H_4-(CH_2)_m-SH$, $m = 1-6$) SAMs on gold and silver surfaces. They concluded that the observed odd−even effect was caused by the differences in coverage.[140,141] Our STM studies reveal the structural origin of such effects.

VI. Mimicking SAM-Based Devices Using STM Measurements

SAMs are promising candidates as active components in molecular electronics.[3,74,142] A major disadvantage in organic molecule-based electronic devices is that the stability and

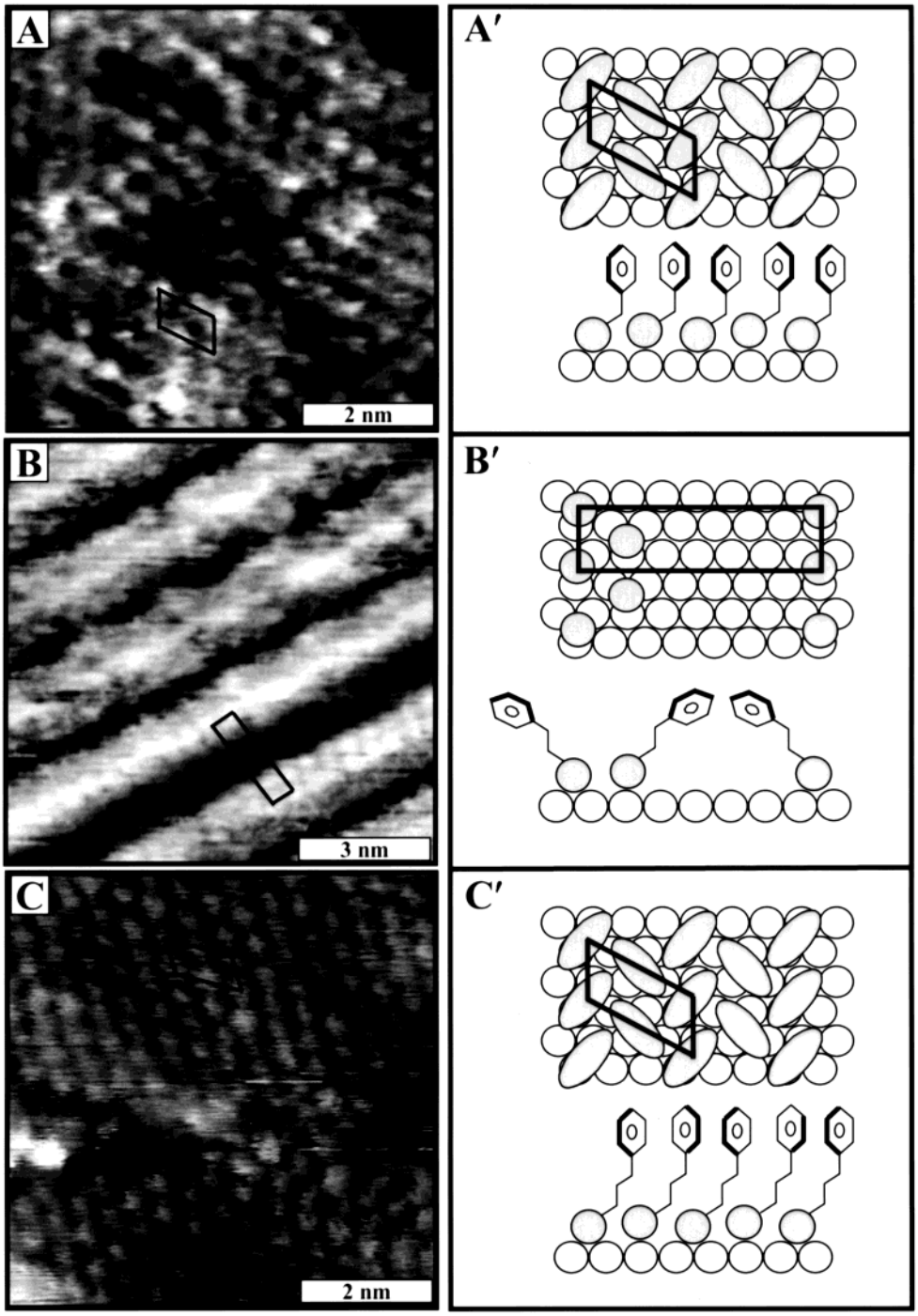

Figure 5. STM topographs of SAMs of (A) 1-phenyl-methanethiol (6 nm × 6 nm), (B) 2-phenyl-ethanethiol (8 nm × 8 nm), and (C) 3-phenyl-propanethiol (6 nm × 6 nm). Top and side views of corresponding structural models are shown in the right-hand column. Both 1-phenyl-methanethiol and 3-phenyl-propanethiol form ordered ($\sqrt{3} \times 2\sqrt{3}$)R30° structures on Au(111). 2-phenyl-ethanethiol monolayers form a (7 × 3) striped structure. Unit cells are indicated both in the images and in the structural models.

robustness of organic systems, in general, are less than their inorganic counterparts. The development of nanoscale insulators and dielectrics,[143] molecular switches, rectifiers, and field-effect transistors require that the organic molecules have sufficient stability against electrical breakdowns. Much effort has been devoted into using various organic molecules to form SAMs with the desired stability and electronic properties.[1,23] STM provides a rapid and precise means to survey the electronic properties, as well as the structure and stability of SAMs, systematically, prior to device fabrication. In addition to high-resolution structural characterization, STM can be used to mimic the interfacial junctions in electronic devices, by regulating tip−surface interactions.

The procedure begins with molecular-level structural characterization. STM images are acquired under low voltage and tunneling current, e.g., 1.0 V and 20 pA for decanethiol SAMs. At a constant current in the picoampere range, increasing the bias voltage results in an increase in the electric field applied between the tip and the surface. The electronic characteristics of SAMs are studied by taking $I-V$ measurements, whereas the structural integrity of SAMs under the tip are monitored in situ by acquiring high-resolution images.

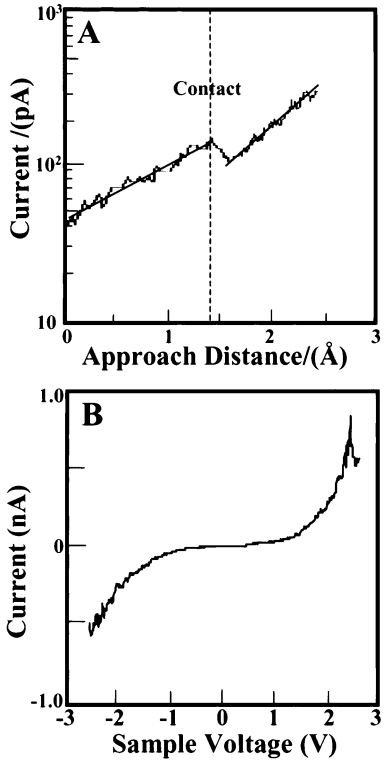

Figure 6. Scanning tunneling spectroscopy of decanethiol SAMs on Au(111). Panel A shows a typical current−distance ($I-Z$) curve of decanethiol SAMs measured from the setpoint (I = 50 pA and V = 1.0 V). The setpoint is used as the reference position (Z = 0). The contact between the tip and the monolayer surface is defined as the first kink point on the ln(I)−Z curve, indicated by the vertical dashed line. Panel B shows the $I-V$ characteristic of decanethiol SAMs when the tip is in contact with the SAM surface. At 2.4 V (sample positive), a peak with a negative differential resistance is observed.

To mimic a device junction, the STM tip is precisely positioned in contact with the termini of SAMs. This positioning is achieved by first examining the $I-Z$ curve, as shown in Figure 6A. Prior to the tip−SAM surface contact, the ln(I)−Z relationship increases linearly as the tip approaches the surface. The tunneling barrier height, Φ, can be calculated using

$$\Phi = -0.952\left[\frac{\Delta \ln(I)}{\Delta Z}\right]^2 \quad (1)$$

where I is the tunneling current and Z is the tip−surface separation.[144−146] After contact, the tunneling current continues to increase linearly, with a larger slope, as the tip penetrates into the SAM. The first turning point (indicated in Figure 6A) defines the tip−methyl group contact position, at which $I-V$ curves are acquired, as shown in Figure 6B. $I-V$ curves obtained in this manner most accurately reflect the electronic characteristics of SAMs in a device junction. Figure 6B shows a typical $I-V$ curve of a decanethiol SAM at contact, for a voltage range of −2.5 to +2.5 V. The curve was acquired as the voltage was swept from a negative sample bias to a positive one. The $I-V$ curve shows that the current was almost symmetric and linear at very low voltage and increased exponentially at higher voltages. Two important observations are obtained from the $I-V$ measurements: (i) at ∼2.4 V or beyond (sample positive), a peak occurs, corresponding to a negative differential resistance ($dV/dI < 0$, or NDR); and (ii) the $I-V$ profile is not completely symmetric at large voltages. Although the curve can extend down to a negative sample bias of −10 V, it is difficult to obtain stable $I-V$ measurements beyond +2.5 V, because of the occurrence of current spikes. Current spikes indicate that the devices break down.

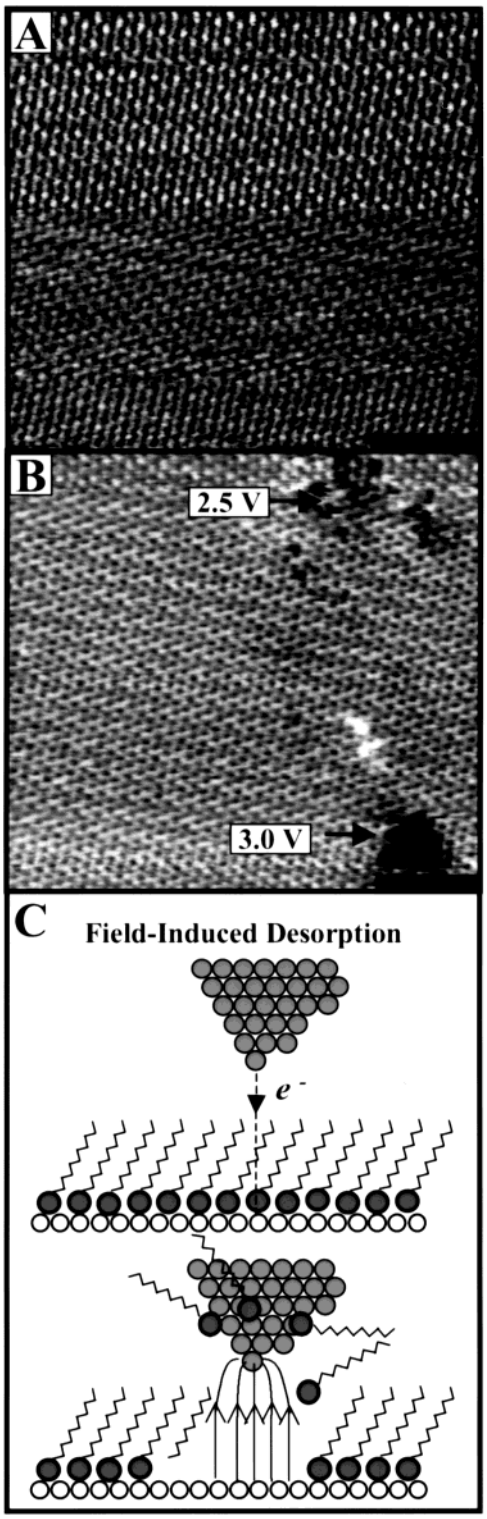

Figure 7. STM-based nanofabrication by field-induced desorption: (A) STM topograph of the decanethiol monolayer obtained before application of the threshold field and (B) STM image acquired after fabrication. At 2.5 V, few molecular vacancies are created. At 3.0 V, a hole of 3 nm in diameter is produced. Panel C shows a schematic diagram of the field-induced desorption procedure. Scale bars in panels A and B are 5 nm.

In previous studies, observations of NDR for SAM-based junctions have been attributed to tip−molecule interactions or resonant tunneling, i.e., narrow features in the local density of

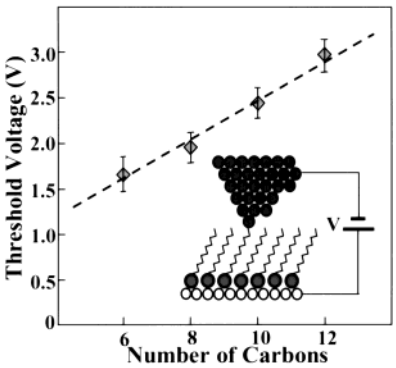

Figure 8. Threshold voltage as a function of the number of C atoms in the alkyl chains. Measurements were conducted at the tip−SAM contact point. The straight dashed line represents the least-squares fit, with a slope of 1.9×10^9 V/m.

states of the tip apex with the surface.[129,147,148] The breakdown voltage of SAMs was attributed to an electronic process, although the mechanism was not known.[149−151] To verify and explore the mechanism of the breakdown voltage, we have imaged thiols before, during, and after $I-V$ measurements. Molecular-resolution STM topographs reveal that the surface of decanethiol SAMs undergoes little change below +2.5 V, as shown in Figure 7A. By increasing the voltage to +2.5 V, dark holes were generated, as shown in Figure 7B. The depth of these holes is 7 Å, indicating a desorption of decanethiol molecules. At a higher voltage of 3.0 V, a larger hole (3 nm in diameter) is produced, corresponding to the removal of ∼32 decanethiol molecules. Most of the removed molecules were attached to the STM tips, because we observed that continuous scanning will heal the holes and that materials from the STM tips readsorb onto designated areas with voltage pulsing. Therefore, we conclude that NDR is caused by a local structural change, i.e., the desorption of the decanethiol molecules under the tip, instead of unknown electronic processes. This mechanism should be considered for the design of future SAM-based devices.

The observation of a breakdown voltage (+2.5 V) may be rationalized by the mechanism of field-induced dissociation and desorption.[152−157] From a qualitative perspective, breakdown only occurs at a sufficiently large positive bias, not at the reversed polarity, which indicates that it is the effect of an electric field. The electric field measured at the point of breakdown is $\sim 1.8 \times 10^9$ V/m for decanethiol SAMs with a thickness of 1.34 nm. Additional evidence was collected by investigation of the threshold voltage as a function of the chain length or the number of C atoms in alkanethiol SAMs. Figure 8 shows a linear relationship between the electric field as a function of the number of C atoms. The slope of the line corresponds to a field strength of 1.9×10^9 V/m, which is similar in magnitude to the breakdown electric fields observed by Wold et al. in conductive AFM studies,[150] and by Hagg et al. in electric breakdown measurements for Hg/SAM/Ag junctions.[149] In thiol SAMs, the partial negative charge for sulfur has been calculated to be $\sim 0.4\ e^-$.[158] The S−Au separation is 2.2 Å. The S−Au dipole moment (μ) is $\sim 8.4 \times 10^{-30}$ C m (or 2.5 D).[74] For a positive bias, the S−Au bond is weakened, because the electrical field forces the charge to redistribute, i.e., a reduction of the partial charges on S and Au atoms occurs. If the electric field is sufficiently large, the partial charges diminish, leading to the dissociation of S−Au bonds. Analogous observations have been found, such as the dissociation of Si−NO bonds under a threshold electric field of $\sim 1.2 \times 10^9$ V/m.[157] Using ab initio density functional cluster theory, the charge

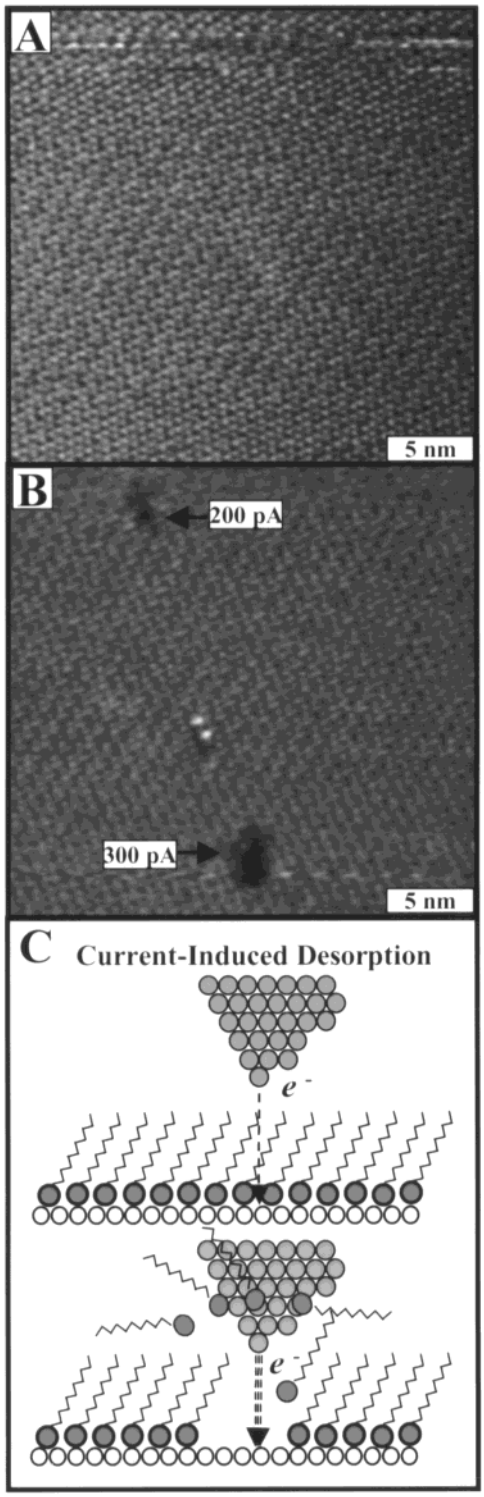

Figure 9. Current-induced desorption by scanning tunneling microscopy (STM). Images of a decanethiol SAM were obtained (A) before and (B) after fabrication. A 1-nm hole was fabricated at +1.0 V and 200 pA, and a hole 3 nm in diameter was formed at 300 pA. Panel C shows a schematic diagram of the desorption procedure using tunneling electrons.

redistribution is predicted to occur under a high positive local field, which breaks chemical bonds.[156] In addition to understanding the electrical behavior of SAMs under an electric field, systematic $I-V$ studies suggest a procedure for nanofabrication or molecule manipulation using STM, as shown in Figure 7C. The electrical field is local; therefore, up to molecular precision

can be achieved in surface fabrication. The newly produced nanostructures can also be characterized and modified in situ.

For comparison to the field-induced mechanism, nanofabrication using tunneling current is shown in Figure 9. First, the SAMs are imaged at 1 V and 10−20 pA to select a fabrication location (Figure 9A). While keeping the voltage constant and the feedback active, the tunneling current is gradually increased by moving the tip toward the surface. The $I-Z$ curve follows an exponential relationship, as dictated in quantum tunneling processes, until the current reaches the fabrication threshold, at which point a large fluctuation of current is observed.[61] The fluctuation is attributed to the movements of atoms and molecules within the tunneling junction, e.g., the desorption of thiol molecules. At 200 pA, holes as small as 1 nm in diameter can be produced at 1 V (Figure 9B). In a nearby location, a 3-nm hole was produced at a higher tunneling current, e.g., 300 pA. The corresponding cursor profiles reveal the depth of the holes to be 0.7 ± 0.2 nm. This observed apparent depth is greater than a single Au(111) step (0.24 nm) but is smaller than the thickness of decanethiol SAMs (1.34 nm). This observation is consistent with previous STM studies and the fact that alkyl chains do not make a significant contribution to the tunneling current. The electronic density of states of hydrocarbon chains is sufficiently distant from the Fermi levels of the tungsten tip and the gold substrate. With the presence of clean tungsten or platinum−rhodium tips, the thiols that are loosely bonded to the gold surface could attach to the tips. The current-induced desorption procedure is illustrated in Figure 9C.

Tunneling-current-induced desorption can be understood by the following contributions. First, the local electric field causes the redistribution of charges at the S−Au bonds. Because the corresponding electric field is estimated to be $\sim 8 \times 10^8$ V/m, which is smaller than the threshold field strength of 1.9×10^9 V/m, the charge redistribution weakens the S−Au bonds but is insufficient for bond dissociation. The contribution from the field is supported by our observation that a positive bias is required. At negative sample voltages of −1 to −4 V, no observable desorption was evident, even at 1 nA. The second contribution is from the tunneling current. Tunneling electrons are known to cause the dissociation of chemical bonds. A proposed model is the vibrational excitation of adsorbate molecules by resonant inelastic electron tunneling.[159−161] With the weakening of S−Au bonds by local fields, a tunneling current as low as 70 pA can induce desorption at a voltage of 2.0 V.

VII. Concluding Remarks

Organothiol self-assembled monolayers (SAMs) on gold surfaces provide a relatively simple approach to modify interfacial properties in the design of organic molecular devices. The structures of alkanethiol SAMs have been characterized by scanning tunneling microscopy (STM) with molecular resolution, which reveals the packing, periodicity, morphology, and defects. Molecular-level structural characterization provides a fundamental understanding of interfacial properties, such as passivation, wettability, and lubricity. In addition to structural characterization, STM is proven to be a powerful tool in monitoring the process of self-assembly and thermal annealing. The concept of regulating and controlling interfacial properties by introducing various functional groups is validated, although further work remains to correlate the structure and property systematically. Investigations included in this article have revealed the importance of a molecular-level understanding in realizing SAM-based electronic devices. If SAMs were to be used in microelectromechanical systems (MEMS), nanoelectromechanical systems (NEMS), and molecular devices, molecular- and nanoscopic-level defects, such as adatom and vacancy islands, become a significant factor. The formation mechanism of adatom and vacancy islands has been disclosed. Annealing at temperatures below the melting point can effectively eliminate these defects in alkanethiol SAMs. Structures of SAMs can be dramatically altered from the parent molecule by the introduction of functionalities such as phenyl groups into alkanethiols.

STM tip−surface interactions can be tuned to mimic the interfacial junctions in molecular devices effectively. Combining structural characterization with $I-V$ measurements is critical for understanding the electronic properties of molecular devices, for device design, as well as for avoiding possible misassignments of electronic behavior. Taking advantage of the high local electric field and tunneling current, STM tips have proven to be an effective tool for molecular manipulation or nanofabrication with molecular-level precision. The resulting nanostructures can be characterized and modified in situ.

We believe that extensive work and exciting opportunities lay ahead in the field of SAM-based electronic devices and in the modification of interfacial properties. Three specific areas are particularly interesting in our view: (i) the introduction of specific functional groups to meet the design criteria for electronic properties in molecular devices; (ii) nanofabrication using STM; and (iii) control of the biological properties such as protein adhesion by designing proper molecular precursors and engineering their arrangement on surfaces at a molecular level. We anticipate the development of new techniques (e.g., nanofabrication methodology) and revelations of new scientific insights in the pursuit of these research areas.

Acknowledgment. *We dedicate this work in memory of Dr. G. E. Poirier, for his extraordinary contributions to STM studies of SAMs, which have revolutionized our understanding of organic thin films and the STM imaging mechanism.* We thank Professor A. Ulman (New York Polytechnic University) and Professor L. R. Sita (University of Maryland) for providing 4-chloro-4′-mercaptobipheny and 4-[4′-(phenylethynyl)-phenylethynyl]-benzenethiol compounds, respectively. Helpful discussions and technical assistance from Dr. Thomas Jung (Paul Scherrer Institute) and J. C. Garno and Y. Qian (Wayne State University) are highly appreciated. We also acknowledge both reviewers for their suggestions and persistence in enhancing the clarity of the manuscript; the second reviewer specifically noted the importance of the mobility of thiols upon chemisorption on gold, which is one of the main sources of vacancy island formation. This work is supported by the University of California at Davis and the National Science Foundation (NSF) (through Grant No. CHE-9733410, Grant No. CHE-0244830, and the Stanford University−CPIMA program).

References and Notes

(1) Tour, J. M. *Acc. Chem. Res.* **2000**, *33*, 791.
(2) Joachim, C.; Gimzewski, J. K.; Aviram, A. *Nature* **2000**, *408*, 541.
(3) Reed, M. A. *Proc. IEEE* **1999**, *87*, 652.
(4) Pease, A. R.; Jeppesen, J. O.; Stoddart, J. F.; Luo, Y.; Collier, C. P.; Heath, J. R. *Acc. Chem. Res.* **2001**, *34*, 433.
(5) de Boer, M. P.; Mayer, T. M. *MRS Bull.* **2001**, *26*, 302.
(6) Maboudian, R.; Ashurst, W. R.; Carraro, C. *Tribol. Lett.* **2002**, *12*, 95.
(7) Komvopoulos, K. *Wear* **1996**, *200*, 305.
(8) Komvopoulos, K.; Yan, W. *J. Tribol.* **1997**, *119*, 391.
(9) Alivisatos, A. P.; Barbara, P. F.; Castleman, A. W.; Chang, J.; Dixon, D. A.; Klein, M. L.; McLendon, G. L.; Miller, J. S.; Ratner, M. A.; Rossky, P. J.; Stupp, S. I.; Thompson, M. E. *Adv. Mater.* **1998**, *10*, 1297.

(10) Crooks, R. M.; Ricco, A. J. *Acc. Chem. Res.* **1998**, *31*, 219.
(11) Flink, S.; van Veggel, F.; Reinhoudt, D. N. *Adv. Mater.* **2000**, *12*, 1315.
(12) Willner, I.; Katz, E. *Angew. Chem.−Int. Ed.* **2000**, *39*, 1180.
(13) Bishop, A. R.; Nuzzo, R. G. *Curr. Opin. Colloid Interface Sci.* **1996**, *1*, 127.
(14) Prime, K. L.; Whitesides, G. M. *Science* **1991**, *252*, 1164.
(15) Prime, K. L.; Whitesides, G. M. *J. Am. Chem. Soc.* **1993**, *115*, 10714.
(16) Mrksich, M.; Chen, C. S.; Xia, Y. N.; Dike, L. E.; Ingber, D. E.; Whitesides, G. M. *Proc. Natl. Acad. Sci. U.S.A.* **1996**, *93*, 10775.
(17) Deng, L.; Mrksich, M.; Whitesides, G. M. *J. Am. Chem. Soc.* **1996**, *118*, 5136.
(18) Wadu-Mesthrige, K.; Amro, N. A.; Liu, G. Y. *Scanning* **2000**, *22*, 380.
(19) Wadu-Mesthrige, K.; Amro, N. A.; Garno, J. C.; Xu, S.; Liu, G. Y. *Biophys. J.* **2001**, *80*, 1891.
(20) Liu, G. Y.; Amro, N. A. *Proc. Natl. Acad. Sci. U.S.A.* **2002**, *99*, 5165.
(21) Ulman, A. *Acc. Chem. Res.* **2001**, *34*, 855.
(22) Carpick, R. W.; Salmeron, M. *Chem. Rev.* **1997**, *97*, 1163.
(23) Fendler, J. H. *Chem. Mater.* **2001**, *13*, 3196.
(24) Zhu, X. Y. *Annu. Rev. Phys. Chem.* **2002**, *53*, 221.
(25) Dubois, L. H.; Nuzzo, R. G. *Annu. Rev. Phys. Chem.* **1992**, *43*, 437.
(26) Ulman, A. *Chem. Rev.* **1996**, *96*, 1533.
(27) Schreiber, F. *Prog. Surf. Sci.* **2000**, *65*, 151.
(28) Chiang, S. *Chem. Rev.* **1997**, *97*, 1083.
(29) Delamarche, E.; Michel, B.; Biebuyck, H. A.; Gerber, C. *Adv. Mater.* **1996**, *8*, 719.
(30) Poirier, G. E. *Chem. Rev.* **1997**, *97*, 1117.
(31) Haussling, L.; Michel, B.; Ringsdorf, H.; Rohrer, H. *Angew. Chem.−Int. Ed. Engl.* **1991**, *30*, 569.
(32) Edinger, K.; Golzhauser, A.; Demota, K.; Woll, C.; Grunze, M. *Langmuir* **1993**, *9*, 4.
(33) McDermott, C. A.; McDermott, M. T.; Green, J. B.; Porter, M. D. *J. Phys. Chem.* **1995**, *99*, 13257.
(34) Poirier, G. E. *Langmuir* **1997**, *13*, 2019.
(35) Kim, Y. T.; Bard, A. J. *Langmuir* **1992**, *8*, 1096.
(36) Durig, U.; Zuger, O.; Michel, B.; Haussling, L.; Ringsdorf, H. *Phys. Rev. B* **1993**, *48*, 1711.
(37) Camillone, N.; Chidsey, C. E. D.; Liu, G. Y.; Scoles, G. *J. Chem. Phys.* **1993**, *98*, 3503.
(38) Fenter, P.; Eisenberger, P.; Liang, K. S. *Phys. Rev. Lett.* **1993**, *70*, 2447.
(39) Poirier, G. E.; Tarlov, M. J. *Langmuir* **1994**, *10*, 2853.
(40) Delamarche, E.; Michel, B.; Gerber, C.; Anselmetti, D.; Guntherodt, H. J.; Wolf, H.; Ringsdorf, H. *Langmuir* **1994**, *10*, 2869.
(41) Nuzzo, R. G.; Dubois, L. H.; Allara, D. L. *J. Am. Chem. Soc.* **1990**, *112*, 558.
(42) Nuzzo, R. G.; Korenic, E. M.; Dubois, L. H. *J. Chem. Phys.* **1990**, *93*, 767.
(43) Fenter, P.; Eberhardt, A.; Liang, K. S.; Eisenberger, P. *J. Chem. Phys.* **1997**, *106*, 1600.
(44) Whitesides, G. M.; Laibinis, P. E. *Langmuir* **1990**, *6*, 87.
(45) Laibinis, P. E.; Whitesides, G. M. *J. Am. Chem. Soc.* **1992**, *114*, 9022.
(46) Graupe, M.; Koini, T.; Kim, H. I.; Garg, N.; Miura, Y. F.; Takenaga, M.; Perry, S. S.; Lee, T. R. *Mater. Res. Bull.* **1999**, *34*, 447.
(47) Shon, Y. S.; Lee, S.; Colorado, R.; Perry, S. S.; Lee, T. R. *J. Am. Chem. Soc.* **2000**, *122*, 7556.
(48) Lee, S.; Puck, A.; Graupe, M.; Colorado, R.; Shon, Y. S.; Lee, T. R.; Perry, S. S. *Langmuir* **2001**, *17*, 7364.
(49) Ashurst, W. R.; Yau, C.; Carraro, C.; Lee, C.; Kluth, G. J.; Howe, R. T.; Maboudian, R. *Sens. Actuators, A* **2001**, *91*, 239.
(50) Maboudian, R.; Ashurst, W. R.; Carraro, C. *Sens. Actuators A* **2000**, *82*, 219.
(51) Chidsey, C. E. D. *Science* **1991**, *251*, 919.
(52) Smalley, J. F.; Feldberg, S. W.; Chidsey, C. E. D.; Linford, M. R.; Newton, M. D.; Liu, Y. P. *J. Phys. Chem.* **1995**, *99*, 13141.
(53) Sikes, H. D.; Smalley, J. F.; Dudek, S. P.; Cook, A. R.; Newton, M. D.; Chidsey, C. E. D.; Feldberg, S. W. *Science* **2001**, *291*, 1519.
(54) Bumm, L. A.; Arnold, J. J.; Dunbar, T. D.; Allara, D. L.; Weiss, P. S. *J. Phys. Chem. B* **1999**, *103*, 8122.
(55) Xu, S.; Liu, G. Y. *Langmuir* **1997**, *13*, 127.
(56) Piner, R. D.; Zhu, J.; Xu, F.; Hong, S. H.; Mirkin, C. A. *Science* **1999**, *283*, 661.
(57) Xia, Y. N.; Whitesides, G. M. *Annu. Rev. Mater. Sci.* **1998**, *28*, 153.
(58) Xia, Y. N.; Rogers, J. A.; Paul, K. E.; Whitesides, G. M. *Chem. Rev.* **1999**, *99*, 1823.
(59) Hong, S. H.; Zhu, J.; Mirkin, C. A. *Science* **1999**, *286*, 523.
(60) Amro, N. A.; Xu, S.; Liu, G. Y. *Langmuir* **2000**, *16*, 3006.
(61) Liu, G. Y.; Xu, S.; Qian, Y. L. *Acc. Chem. Res.* **2000**, *33*, 457.
(62) Dhirani, A.; Lin, P. H.; GuyotSionnest, P.; Zehner, R. W.; Sita, L. R. *J. Chem. Phys.* **1997**, *106*, 5249.
(63) Metzger, R. M. *Acc. Chem. Res.* **1999**, *32*, 950.
(64) Collier, C. P.; Wong, E. W.; Belohradsky, M.; Raymo, F. M.; Stoddart, J. F.; Kuekes, P. J.; Williams, R. S.; Heath, J. R. *Science* **1999**, *285*, 391.
(65) Donhauser, Z. J.; Mantooth, B. A.; Kelly, K. F.; Bumm, L. A.; Monnell, J. D.; Stapleton, J. J.; Price, D. W.; Rawlett, A. M.; Allara, D. L.; Tour, J. M.; Weiss, P. S. *Science* **2001**, *292*, 2303.
(66) Andres, R. P.; Bein, T.; Dorogi, M.; Feng, S.; Henderson, J. I.; Kubiak, C. P.; Mahoney, W.; Osifchin, R. G.; Reifenberger, R. *Science* **1996**, *272*, 1323.
(67) Brousseau, L. C.; Zhao, Q.; Shultz, D. A.; Feldheim, D. L. *J. Am. Chem. Soc.* **1998**, *120*, 7645.
(68) Yang, G. H.; Qian, Y. L.; Engtrakul, C.; Sita, L. R.; Liu, G. Y. *J. Phys. Chem. B* **2000**, *104*, 9059.
(69) Kang, J. F.; Ulman, A.; Liao, S.; Jordan, R.; Yang, G. H.; Liu, G. Y. *Langmuir* **2001**, *17*, 95.
(70) Woll, C.; Chiang, S.; Wilson, R. J.; Lippel, P. H. *Phys. Rev. B* **1989**, *39*, 7988.
(71) Chambliss, D. D.; Wilson, R. J.; Chiang, S. *J. Vac. Sci. Technol. B* **1991**, *9*, 933.
(72) Hsung, R. P.; Babcock, J. R.; Chidsey, C. E. D.; Sita, L. R. *Tetrahedron Lett.* **1995**, *36*, 4525.
(73) Hsung, R. P.; Chidsey, C. E. D.; Sita, L. R. *Organometallics* **1995**, *14*, 4808.
(74) Zehner, R. W.; Parsons, B. F.; Hsung, R. P.; Sita, L. R. *Langmuir* **1999**, *15*, 1121.
(75) Qian, Y.; Yang, G.; Yu, J.; Jung, T. A.; Liu, G.-y. *Langmuir* **2003**, *19*, 6056−6065.
(76) Sandy, A. R.; Mochrie, S. G. J.; Zehner, D. M.; Huang, K. G.; Gibbs, D. *Phys. Rev. B* **1991**, *43*, 4667.
(77) Dhirani, A. A.; Zehner, R. W.; Hsung, R. P.; GuyotSionnest, P.; Sita, L. R. *J. Am. Chem. Soc.* **1996**, *118*, 3319.
(78) Duan, L.; Garrett, S. J. *J. Phys. Chem. B* **2001**, *105*, 9812.
(79) Jin, Q.; Rodriguez, J. A.; Li, C. Z.; Darici, Y.; Tao, N. J. *Surf. Sci.* **1999**, *425*, 101.
(80) Hara, M.; Sasabe, H.; Knoll, W. *Thin Solid Films* **1996**, *273*, 66.
(81) Dhirani, A.; Hines, M. A.; Fisher, A. J.; Ismail, O.; Guyotsionnest, P. *Langmuir* **1995**, *11*, 2609.
(82) Driver, S. M.; Woodruff, D. P. *Langmuir* **2000**, *16*, 6693.
(83) Poirier, G. E. *J. Vac. Sci. Technol. B* **1996**, *14*, 1453.
(84) Kuk, Y.; Silverman, P. J.; Chua, F. M. *J. Microsc. (Oxford)* **1988**, *152*, 449.
(85) Kuk, Y.; Jarrold, M. F.; Silverman, P. J.; Bower, J. E.; Brown, W. L. *Phys. Rev. B* **1989**, *39*, 11168.
(86) Poirier, G. E.; Pylant, E. D. *Science* **1996**, *272*, 1145.
(87) Fitts, W. P.; White, J. M.; Poirier, G. E. *Langmuir* **2002**, *18*, 1561.
(88) Poirier, G. E.; Pylant, E. D. *Langmuir* **2001**, *17*, 1176.
(89) Fitts, W. P.; White, J. M.; Poirier, G. E. *Langmuir* **2002**, *18*, 2096.
(90) Fenter, P.; Eberhardt, A.; Eisenberger, P. *Science* **1994**, *266*, 1216.
(91) Anselmetti, D.; Baratoff, A.; Guntherodt, H. J.; Delamarche, E.; Michel, B.; Gerber, C.; Kang, H.; Wolf, H.; Ringsdorf, H. *Europhys. Lett.* **1994**, *27*, 365.
(92) Delamarche, E.; Michel, B. *Thin Solid Films* **1996**, *273*, 54.
(93) Poirier, G. E.; Tarlov, M. J.; Rushmeier, H. E. *Langmuir* **1994**, *10*, 3383.
(94) Cavalleri, O.; Hirstein, A.; Kern, K. *Surf. Sci.* **1995**, *340*, L960.
(95) Poirier, G. E.; Tarlov, M. J. *J. Phys. Chem.* **1995**, *99*, 10966.
(96) Delamarche, E.; Michel, B.; Kang, H.; Gerber, C. *Langmuir* **1994**, *10*, 4103.
(97) Camillone, N.; Eisenberger, P.; Leung, T. Y. B.; Schwartz, P.; Scoles, G.; Poirier, G. E.; Tarlov, M. J. *J. Chem. Phys.* **1994**, *101*, 11031.
(98) Sette, F.; Hashizume, T.; Comin, F.; Macdowell, A. A.; Citrin, P. H. *Phys. Rev. Lett.* **1988**, *61*, 1384.
(99) Trevor, D. J.; Chidsey, C. E. D.; Loiacono, D. N. *Phys. Rev. Lett.* **1989**, *62*, 929.
(100) Zehner, R. W.; Sita, L. R. *Langmuir* **1997**, *13*, 2973.
(101) Lin, P. H.; Guyot-Sionnest, P. *Langmuir* **1999**, *15*, 6825.
(102) Kondoh, H.; Kodama, C.; Nozoye, H. *J. Phys. Chem. B* **1998**, *102*, 2310.
(103) Kondoh, H.; Kodama, C.; Sumida, H.; Nozoye, H. *J. Chem. Phys.* **1999**, *111*, 1175.
(104) Whelan, C. M.; Barnes, C. J.; Gregoire, C.; Pireaux, J. J. *Surf. Sci.* **2000**, *454*, 67.
(105) Lavrich, D. J.; Wetterer, S. M.; Bernasek, S. L.; Scoles, G. *J. Phys. Chem. B* **1998**, *102*, 3456.
(106) Wetterer, S. M.; Lavrich, D. J.; Cummings, T.; Bernasek, S. L.; Scoles, G. *J. Phys. Chem. B* **1998**, *102*, 9266.
(107) Leung, T. Y. B.; Gerstenberg, M. C.; Lavrich, D. J.; Scoles, G.; Schreiber, F.; Poirier, G. E. *Langmuir* **2000**, *16*, 549.

(108) Leung, T. Y. B.; Schwartz, P.; Scoles, G.; Schreiber, F.; Ulman, A. *Surf. Sci.* **2000**, *458*, 34.
(109) Kang, J.; Rowntree, P. A. *Langmuir* **1996**, *12*, 2813.
(110) Truong, K. D.; Rowntree, P. A. *J. Phys. Chem.* **1996**, *100*, 19917.
(111) Xiao, X. D.; Hu, J.; Charych, D. H.; Salmeron, M. *Langmuir* **1996**, *12*, 235.
(112) Noy, A.; Frisbie, C. D.; Rozsnyai, L. F.; Wrighton, M. S.; Lieber, C. M. *J. Am. Chem. Soc.* **1995**, *117*, 7943.
(113) Salmeron, M. *Tribol. Lett.* **2001**, *10*, 69.
(114) Kiely, J. D.; Houston, J. E.; Mulder, J. A.; Hsung, R. P.; Zhu, X. Y. *Tribol. Lett.* **1999**, *7*, 103.
(115) Sachs, S. B.; Dudek, S. P.; Hsung, R. P.; Sita, L. R.; Smalley, J. F.; Newton, M. D.; Feldberg, S. W.; Chidsey, C. E. D. *J. Am. Chem. Soc.* **1997**, *119*, 10563.
(116) Campbell, I. H.; Rubin, S.; Zawodzinski, T. A.; Kress, J. D.; Martin, R. L.; Smith, D. L.; Barashkov, N. N.; Ferraris, J. P. *Phys. Rev. B* **1996**, *54*, 14321.
(117) Vilan, A.; Cahen, D. *Trends Biotechnol.* **2002**, *20*, 22.
(118) Campbell, I. H.; Kress, J. D.; Martin, R. L.; Smith, D. L.; Barashkov, N. N.; Ferraris, J. P. *Appl. Phys. Lett.* **1997**, *71*, 3528.
(119) Vilan, A.; Shanzer, A.; Cahen, D. *Nature* **2000**, *404*, 166.
(120) Tour, J. M.; Jones, L.; Pearson, D. L.; Lamba, J. J. S.; Burgin, T. P.; Whitesides, G. M.; Allara, D. L.; Parikh, A. N.; Atre, S. V. *J. Am. Chem. Soc.* **1995**, *117*, 9529.
(121) Tour, J. M.; Rawlett, A. M.; Kozaki, M.; Yao, Y. X.; Jagessar, R. C.; Dirk, S. M.; Price, D. W.; Reed, M. A.; Zhou, C. W.; Chen, J.; Wang, W. Y.; Campbell, I. *Chem.—Eur. J.* **2001**, *7*, 5118.
(122) Hong, S.; Reifenberger, R.; Tian, W.; Datta, S.; Henderson, J. I.; Kubiak, C. P. *Superlattices Microstruct.* **2000**, *28*, 289.
(123) Bumm, L. A.; Arnold, J. J.; Cygan, M. T.; Dunbar, T. D.; Burgin, T. P.; Jones, L.; Allara, D. L.; Tour, J. M.; Weiss, P. S. *Science* **1996**, *271*, 1705.
(124) Reed, M. A.; Zhou, C.; Muller, C. J.; Burgin, T. P.; Tour, J. M. *Science* **1997**, *278*, 252.
(125) Tian, W. D.; Datta, S.; Hong, S. H.; Reifenberger, R.; Henderson, J. I.; Kubiak, C. P. *J. Chem. Phys.* **1998**, *109*, 2874.
(126) Ishida, T.; Mizutani, W.; Choi, N.; Akiba, U.; Fujihira, M.; Tokumoto, H. *J. Phys. Chem. B* **2000**, *104*, 11680.
(127) Ishida, T.; Mizutani, W.; Aya, Y.; Ogiso, H.; Sasaki, S.; Tokumoto, H. *J. Phys. Chem. B* **2002**, *106*, 5886.
(128) Wold, D. J.; Haag, R.; Rampi, M. A.; Frisbie, C. D. *J. Phys. Chem. B* **2002**, *106*, 2813.
(129) Fan, F. R. F.; Yang, J. P.; Cai, L. T.; Price, D. W.; Dirk, S. M.; Kosynkin, D. V.; Yao, Y. X.; Rawlett, A. M.; Tour, J. M.; Bard, A. J. *J. Am. Chem. Soc.* **2002**, *124*, 5550.
(130) Kergueris, C.; Bourgoin, J. P.; Palacin, S.; Esteve, D.; Urbina, C.; Magoga, M.; Joachim, C. *Phys. Rev. B* **1999**, *59*, 12505.
(131) Tao, Y. T.; Wu, C. C.; Eu, J. Y.; Lin, W. L. *Langmuir* **1997**, *13*, 4018.
(132) Chang, S. C.; Chao, I.; Tao, Y. T. *J. Am. Chem. Soc.* **1994**, *116*, 6792.
(133) Sabatani, E.; Cohenboulakia, J.; Bruening, M.; Rubinstein, I. *Langmuir* **1993**, *9*, 2974.
(134) Jung, H. H.; Do Won, Y.; Shin, S.; Kim, K. *Langmuir* **1999**, *15*, 1147.
(135) Staub, R.; Toerker, M.; Fritz, T.; Schmitz-Hubsch, T.; Sellam, F.; Leo, K. *Langmuir* **1998**, *14*, 6693.
(136) Duan, L. L.; Garrett, S. J. *Langmuir* **2001**, *17*, 2986.
(137) Laibinis, P. E.; Whitesides, G. M.; Allara, D. L.; Tao, Y. T.; Parikh, A. N.; Nuzzo, R. G. *J. Am. Chem. Soc.* **1991**, *113*, 7152.
(138) Walczak, M. M.; Chung, C. K.; Stole, S. M.; Widrig, C. A.; Porter, M. D. *J. Am. Chem. Soc.* **1991**, *113*, 2370.
(139) Tao, Y. T.; Lee, M. T.; Chang, S. C. *J. Am. Chem. Soc.* **1993**, *115*, 9547.
(140) Rong, H. T.; Frey, S.; Yang, Y. J.; Zharnikov, M.; Buck, M.; Wuhn, M.; Woll, C.; Helmchen, G. *Langmuir* **2001**, *17*, 1582.
(141) Heister, K.; Rong, H. T.; Buck, M.; Zharnikov, M.; Grunze, M.; Johansson, L. S. O. *J. Phys. Chem. B* **2001**, *105*, 6888.
(142) Tour, J. M.; Reinerth, W. A.; Jones, L.; Burgin, T. P.; Zhou, C. W.; Muller, C. J.; Deshpande, M. R.; Reed, M. A. Recent Advances in Molecular Scale Electronics. In *Molecular Electronics: Science and Technology*, Annals of the New York Academy of Sciences 852; New York Academy of Sciences: New York, 1998; p 197.
(143) Rampi, M. A.; Schueller, O. J. A.; Whitesides, G. M. *Appl. Phys. Lett.* **1998**, *72*, 1781.
(144) Gimzewski, J. K.; Moller, R. *Phys. Rev. B* **1987**, *36*, 1284.
(145) Olesen, L.; Brandbyge, M.; Sorensen, M. R.; Jacobsen, K. W.; Laegsgaard, E.; Stensgaard, I.; Besenbacher, F. *Phys. Rev. Lett.* **1996**, *76*, 1485.
(146) Olesen, L.; Laegsgaard, E.; Stensgaard, I.; Besenbacher, F. *Appl. Phys. A: Mater. Sci. Process.* **1998**, *66*, S157.
(147) Xue, Y. Q.; Datta, S.; Hong, S.; Reifenberger, R.; Henderson, J. I.; Kubiak, C. P. *Phys. Rev. B* **1999**, *59*, R7852.
(148) Chen, J.; Reed, M. A.; Rawlett, A. M.; Tour, J. M. *Science* **1999**, *286*, 1550.
(149) Haag, R.; Rampi, M. A.; Holmlin, R. E.; Whitesides, G. M. *J. Am. Chem. Soc.* **1999**, *121*, 7895.
(150) Wold, D. J.; Frisbie, C. D. *J. Am. Chem. Soc.* **2001**, *123*, 5549.
(151) Cui, X. D.; Zarate, X.; Tomfohr, J.; Sankey, O. F.; Primak, A.; Moore, A. L.; Moore, T. A.; Gust, D.; Harris, G.; Lindsay, S. M. *Nanotechnology* **2002**, *13*, 5.
(152) Lyo, I. W.; Avouris, P. *Science* **1991**, *253*, 173.
(153) Avouris, P.; Lyo, I. W. *Appl. Surf. Sci.* **1992**, *60−61*, 426.
(154) Avouris, P.; Walkup, R. E.; Rossi, A. R.; Akpati, H. C.; Nordlander, P.; Shen, T. C.; Abeln, G. C.; Lyding, J. W. *Surf. Sci.* **1996**, *363*, 368.
(155) Akpati, H. C.; Nordlander, P.; Lou, L.; Avouris, P. *Surf. Sci.* **1997**, *372*, 9.
(156) Akpati, H. C.; Nordlander, P.; Lou, L.; Avouris, P. *Surf. Sci.* **1998**, *401*, 47.
(157) Rezaei, M. A.; Stipe, B. C.; Ho, W. *J. Chem. Phys.* **1999**, *110*, 4891.
(158) Sellers, H.; Ulman, A.; Shnidman, Y.; Eilers, J. E. *J. Am. Chem. Soc.* **1993**, *115*, 9389.
(159) Stipe, B. C.; Rezaei, M. A.; Ho, W.; Gao, S.; Persson, M.; Lundqvist, B. I. *Phys. Rev. Lett.* **1997**, *78*, 4410.
(160) Ho, W. *Acc. Chem. Res.* **1998**, *31*, 567.
(161) Lorente, N.; Persson, M. *Faraday Discuss.* **2000**, 277.